

Ultrasonic Detection of Disbond Defects in Steel-Epoxy-Steel Sandwich Structures

Zhifei Xiao,^{1,2} Shuying Tang,³ Han Jiang,^{1,2} Jing Rao,^{1,2} Limei Fan,^{2,4} Zhiqiang Cheng,⁵
Rongguang Li,⁶ and Ling Sun⁶

¹Hangzhou International Innovation Institute, Beihang University, Hangzhou, China

²Key Laboratory of Precision Opto-mechatronics Technology of Education Ministry, School of Instrumentation and Opto-Electronic Engineering, Beihang University, Beijing, China

³Beijing Intellectual Property Protection Center, Beijing, China

⁴Shandong Nonmetallic Materials Institute, Jinan, China

⁵School of Mechanics and Aerospace Engineering, Southwest Jiaotong University, Chengdu, China

⁶PipeChina north Pipeline Company, Langfang, Hebei, China

(Received 29 April 2025; Revised 18 May 2025; Accepted 08 June 2025; Published online 11 June 2025)

Abstract: The steel-epoxy-steel sandwich structures provide enhanced corrosion resistance and fatigue resistance, making them suitable for pipeline rehabilitation with effective repair and long-term durability. However, the repair quality can be compromised by disbond between the steel and epoxy layers, which may result from insufficient epoxy injection. Conventional ultrasonic testing faces challenges in accurately locating disbond defects due to aliased echo interference at interfaces. This paper proposes a signal processing algorithm for improving the accuracy of ultrasonic reflection method for detecting disbond defects between steel and epoxy layers. First, a coati optimization algorithm-variational mode decomposition (COA-VMD) is applied to adaptively decompose the ultrasonic signals and extract the intrinsic mode function components that show high correlation with the defect-related signals. Then, by calculating the relative reflectance at the interface and establishing a quantitative evaluation index based on acoustic impedance discontinuity, the locations of disbond defects are identified. Experimental results demonstrate that this method can effectively detect the locations of disbond defects between steel and epoxy layers.

Keywords: disbond detection; sandwich structures; ultrasonic testing; variational mode decomposition

I. INTRODUCTION

With the increasing operational lifespan of global energy pipeline networks, aging infrastructure has led to severe challenges, such as corrosion and leakage, posing significant risks to industrial safety and environmental sustainability [1,2]. In situ rehabilitation utilizing steel-epoxy-steel sandwich structures has emerged as a key strategy for maintaining pipeline integrity. Among various reinforcement techniques, this structure has gained widespread application in oil and gas pipeline rehabilitation due to its exceptional sealing performance, corrosion resistance, and mechanical reinforcement capabilities [3]. This technology relies on epoxy injection to achieve interlayer bonding; however, disbond defects often occur in practical engineering applications due to factors such as temperature fluctuations, insufficient injection pressure, and uneven distribution [4]. These disbond defects can result in a loss of interlayer bonding strength and lead to localized stress concentration under operational loads, which critically compromise the structural integrity and service life of rehabilitated pipelines [5]. Therefore, detection of disbond defects is crucial for evaluating the quality of pipeline rehabilitation and ensuring long-term operational reliability.

As a conventional non-destructive testing (NDT) technique, ultrasonic NDT is employed in the inspection of multi-layer structures [6,7]. It utilizes high-frequency

mechanical vibrations to transfer energy, and the ultrasonic wave propagates through the materials until it encounters an interface with discontinuity. The sudden change in acoustic impedance between different materials causes a portion of the incident ultrasonic wave to be reflected, producing an observable reflection signal [8]. By capturing and analyzing the characteristics of the reflected waves, such as amplitude, it is possible to assess the quality of bonding within sandwich structures.

Wang *et al.* [9] derived expressions for ultrasonic longitudinal and shear wave transmission and reflection coefficients in layered media using spring models and established boundary conditions for the interfaces based on the transfer matrix method. The experimental results are basically consistent with numerical solution results, providing a theoretical foundation for ultrasonic inspection of bonding interfaces of aluminum and polymethyl methacrylate. Hou *et al.* [10] proposed an ultrasonic resonance to evaluate the bonding between ultra-thin nickel sheets and silicone films. By analyzing the attenuation characteristics of ultrasonic resonance signals under different bonding conditions, they defined a bonding coefficient to quantify the strength of interfacial adhesion. Experimental results demonstrated that bonding quality could be effectively distinguished by setting appropriate thresholds. However, due to the limitation of experimental conditions, the specific relationship between adhesion coefficient and defects has not been established. Sergey *et al.* [11] present an ultrasonic pulse-echo method for detecting disbonds at the interfaces

Corresponding author: Jing Rao (e-mail: jingrao@buaa.edu.cn).

of adhesively bonded joints in automotive assemblies. The method decomposes ultrasonic waveforms to isolate reflections from both metal-adhesive interfaces. By employing a reference waveform acquired from a bare metal sheet, it effectively suppresses strong reverberations in the first metal layer. Experimental validation on steel and aluminum specimens, respectively, demonstrated the technique's ability to detect disbonds via phase inversion of echoes from the second interface. However, this method was only detected in specimens with a thickness of less than 2.5 mm. Challenges faced in the detection of disbond defects in thick-walled steel-epoxy-steel sandwich structures include acoustic energy attenuation, interference from electronic circuit noise, and environmental factors [12,13]. These issues lead to diminished echo amplitudes at critical interfaces, complicating defect identification.

Variational mode decomposition (VMD) is an adaptive signal decomposition method that can simultaneously estimate multiple modes with high efficiency. It is particularly suitable for decomposing and extracting ultrasound signals [14]. Compared to empirical mode decomposition (EMD), VMD avoids redundant components during the decomposition process and significantly reduces the residual noise in individual modes [15]. VMD operates by iteratively searching for the optimal solution to the variational model, determining the center frequencies and bandwidths of each decomposed component, and effectively addressing issues like mode mixing. However, VMD requires considerable effort to determine the optimal number of modes (K) and the penalty factor (α), often through multiple trials, making it computationally intensive [16]. Xu *et al.* [17] proposed a feature extraction method for ultrasonic signals based on improved particle swarm optimization-VMD for detecting cracks in hardwood logs. The method optimizes decomposition parameters using minimum envelope entropy as the fitness function and extracts defect-related features by analyzing the Hilbert marginal spectrum and energy ratios of sub-modes. Although the method is effective in obtaining optimal parameters, it relies on the initial parameter settings. To the best of our knowledge, such signal processing method has not yet been applied to the detection of disbond defects in steel-epoxy thick structures.

To address these limitations, this study uses a coati optimization algorithm-VMD (COA-VMD) framework for adaptive parameter optimization. Dehghani *et al.* [18] proposed the COA, a new population-based intelligent optimization algorithm. The algorithm simulates the natural behaviors of coatis during their predatory attacks on hyenas and evasion from predators to find the optimal solution. Unlike classical intelligent optimization algorithms such as genetic algorithm and particle swarm optimization, COA constructs a mathematical model by mimicking the natural behaviors of coatis. Its search mechanism is divided into two phases: predation and evasion, which provide strong capabilities for both global search and local optimization, and it does not require complex parameter settings. By integrating COA with VMD, the optimal values for K and α are autonomously determined, enabling precise extraction of defect-sensitive frequency components. Based on this, this study further establishes a quantitative evaluation index based on acoustic impedance discontinuity to characterize the location of disbond defects between steel and epoxy layers. The remainder of this paper is organized as follows: Section II presents the COA-VMD algorithm. Section III describes the experimental setup and specimen

configurations. Section IV presents a comparison of the raw and processed signals and gives the results of disbond defect detection, followed by a discussion in Section V. The conclusions are summarized in Section VI.

II. COA-VMD ALGORITHM

A. VMD ALGORITHM

VMD is an adaptive, non-recursive method that achieves signal decomposition through variational optimization, without the need to preset basis functions or wavelet functions [19,20]. By employing variational optimization, VMD breaks down original ultrasonic A-scan signals into several intrinsic mode functions (IMFs), each with a distinct center frequency and finite bandwidth. Each of these IMFs represents a signal with combined frequency and amplitude modulation, which can be expressed as:

$$u_k(t) = A_k(t)\cos(\phi_k(t)), \quad (1)$$

where k represents the number of IMFs, with $k = 1, 2, \dots, K$. $u_k(t)$ denotes the k th IMF; $A_k(t)$ is the instantaneous amplitude of the k th IMF; $\phi_k(t)$ is the phase function of the k th modal component, which typically contains frequency modulation information, indicating how the phase of the signal varies over time.

VMD is to formulate and solve a constrained variational optimization problem. The goal is to identify K modal functions such that the total bandwidth of all decomposed IMFs is minimized, and their sum equals the input source signal [21]. The essential mathematical formula in the VMD is presented in equation (2).

$$\begin{cases} \min_{\{u_k\}, \{\omega_k\}} \left\{ \sum_k \left\| \partial_t \left[\left(\delta(t) + \frac{j}{\pi t} \right) u_k(t) \right] \exp(-j\omega_k t) \right\|_2^2 \right\} \\ \text{s.t.} \left(\sum_k u_k = f \right) \end{cases}, \quad (2)$$

where ∂_t represents the partial derivative with respect to time t , ω_k corresponds to the center frequency, $\delta(t)$ denotes the Dirac delta function, $\left(\delta(t) + \frac{j}{\pi t} \right) u_k(t)$ is the Hilbert transform, the symbols $\|\bullet\|$ represent the norm, respectively, and f denotes the ultrasonic A-scan signals.

The quadratic penalty factor α and the Lagrange multiplier operator λ are introduced to eliminate the constrained behavior of the variational problem as shown in equation (3).

$$\begin{aligned} L_{\{u_k\}, \{\omega_k\}, \lambda} = & \alpha \sum_k \left\| \partial_t \left[\left(\delta(t) + \frac{j}{\pi t} \right) * u_k(t) \right] \exp(-j\omega_k t) \right\|_2^2 \\ & + \left\| f(t) - \sum_k u_k(t) \right\|_2^2 + \left\langle \lambda(t), f(t) - \sum_k u_k(t) \right\rangle, \end{aligned} \quad (3)$$

where L is the augmented Lagrangian, the symbol $\langle \bullet, \bullet \rangle$ represents inner product, and $*$ is the convolution sign. As indicated by equations (2) and (3), the performance of VMD critically depends on two manually configured parameters: the number of decomposition modes K and the penalty factor α . Suboptimal parameter selection may lead to mode redundancy, frequency aliasing, or residual noise, thus necessitating a systematic optimization strategy [22].

B. COA-VMD ALGORITHM

The COA-VMD can automatically determine optimal VMD parameters. This algorithm effectively reduces the potential errors introduced by manual parameter selection while enhancing the computational accuracy. As illustrated in Fig. 1, the COA-VMD process involves: (1) constructing a mathematical model based on coati behavioral simulations and (2) implementing a two-phase search mechanism (predation and evasion phases) that synergistically combines global exploration with local optimization capabilities. Notably, the algorithm operates without requiring complex parameter configurations.

Before using the COA to optimize the parameters of VMD, it is necessary to set the initial parameter ranges, including (1) the population size M (where each coati represents a candidate solution), (2) the maximum iteration number N , and (3) the search boundaries for the target parameters K (mode number) and α (bandwidth control). In this framework, the position vector of the i th coati \mathbf{X}_i ($i=1,2,\dots,M$) is randomly initialized within the defined parameter space, with K and α serving as the optimization targets subject to the termination criterion of reaching either maximum iterations N or convergence thresholds.

$$\mathbf{X}_i = lb + r \cdot (ub - lb), \quad (4)$$

where lb and ub are the lower and upper bounds, respectively, and r is a random number uniformly distributed from 0 to 1.

The fitness of each candidate solution is evaluated by minimizing the envelope entropy. For IMF component u_k , the envelope entropy E_p is calculated as [23]:

$$\begin{cases} E_p = -\sum_{j=1}^N p_j \ln p_j, \\ p_j = \frac{a(j)}{\sum_{m=1}^N a(m)}, \end{cases} \quad (5)$$

where $a(j)$ is the envelope signal obtained from the Hilbert demodulation of the IMF component u_k and p_j is the normalized form of $a(j)$.

In the phase of predation, a computational framework is constructed to emulate the hunting conduct of coatis. The population is evenly divided into two subgroups: one group remains in the trees (keeping the current parameter settings unchanged), while the other group positions itself on the ground to capture prey (actively exploring new parameter combinations). The optimal solution (prey) represents the best parameter combination found so far. The coatis on the ground update their parameter settings based on this optimal solution, meaning they move toward better parameter combinations. For the coatis in the trees, the mathematical expression is:

$$\mathbf{X}_i^{n+1} = \mathbf{X}_i^n + r \cdot (\mathbf{X}_{best}^n - I \cdot \mathbf{X}_i^n), \quad (6)$$

where \mathbf{X}_i^{n+1} is the location information of the i th coati in the $(n+1)$ th iteration; I is a random integer between 1 and 2, and n denotes the current iteration number.

The predation strategy enables coatis to explore diverse locations within the search space, demonstrating COA's global exploration capability in navigating the problem domain. For individuals awaiting prey on the ground, the mathematical expressions are given by:

$$\mathbf{X}_i^{n+1} = \begin{cases} \mathbf{X}_i^n + r \cdot (Iguana^n - I \cdot \mathbf{X}_i^n), & \text{iff } (Iguana^n) < f(\mathbf{X}_i^n) \\ \mathbf{X}_i^n + r \cdot (\mathbf{X}_i^n - Iguana^n), & \text{else} \end{cases} \quad (7)$$

$$Iguana^n = lb + r \cdot (ub - lb), \quad (8)$$

where $f(\mathbf{X}_i^n)$ denotes the fitness value corresponding to the position of the i th raccoon at the n th iteration, and $Iguana^n$ represents the position of the prey that falls from the tree as the optimal parameter combination currently identified during the n th iteration.

The evasion phase is a mathematical model designed to simulate coatis' natural predator-escape behavior. This strategy is triggered when certain coatis exhibit stagnation or regression in their parameter combinations, prompting them to simulate predator evasion by randomly adjusting their parameters to escape potential local optima. This mechanism facilitates exploration of new parameter spaces and enhances global solution discovery. When attacked by a predator, a coati flees from its current position, which is mathematically represented as follows:

$$\begin{cases} lb^{local} = \frac{lb}{n}, \\ ub^{local} = \frac{ub}{n}, \\ \mathbf{X}_i^{n+1} = \mathbf{X}_i^n - (1-2r) \cdot (lb^{local} + r \cdot (ub^{local} - lb^{local})), \end{cases} \quad (9)$$

After each iteration, the population undergoes greedy selection to preserve the highest-performing individuals. The optimal parameters (K -best, α -best) are determined when either the fitness value converges or the maximum iteration count N is reached. Finally, the correlation coefficient between each IMF and the original ultrasonic A-scan signal is calculated. A low correlation coefficient for any given IMF indicates significant noise contamination,

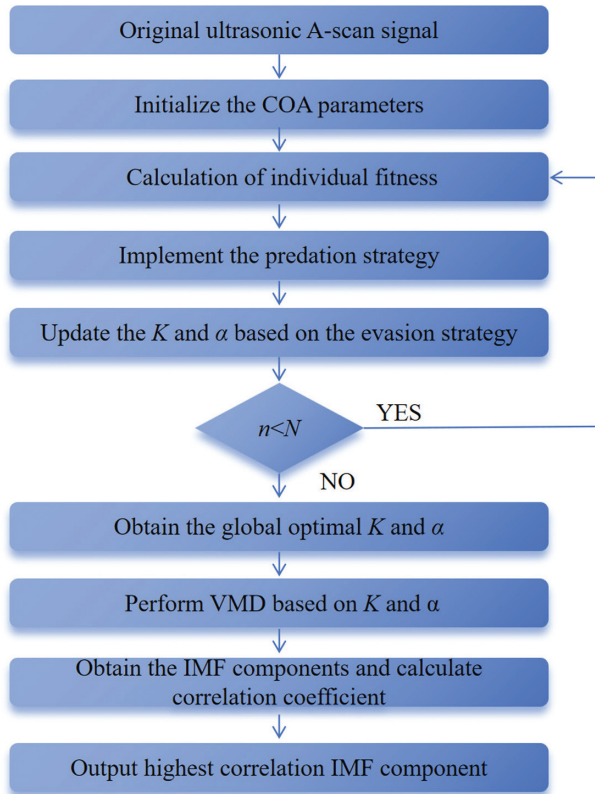


Fig. 1. Flowchart of COA-VMD algorithm.

warranting its removal. The correlation coefficient is calculated as follows [24]:

$$\text{cor}_k = \frac{\sum_{s=1}^S (u_{k,s} - \bar{u}_k)(x_s - \bar{x})}{\sqrt{\sum_{k=1}^K (u_{k,s} - \bar{u}_k)^2} \sqrt{\sum_{k=1}^K (x_s - \bar{x})^2}} \quad (10)$$

where cor_k ($k = 1, 2, \dots, K$) represents the correlation coefficient value for each order IMF, $u_{k,s}$ is the s th data point of the k th IMF component, \bar{u}_k is the mean of the k th IMF component, x is the s th data point of original ultrasonic A-scan signal, and \bar{x} is the mean of the original ultrasonic A-scan signal.

C. DISBOND DEFECT DETECTION OF STEEL-EPOXY LAYERS

To enhance defect detection accuracy, this work employs the COA-VMD algorithm to decompose ultrasonic A-scan signals into their IMF components. The IMF component with the highest correlation is then selected by computing the correlation coefficients of all IMF components using equation (10). Based on the time-domain amplitude characteristics of this highest correlation IMF component, the apparent reflectance is calculated. This reflectance metric serves as the foundation for establishing a disbond defect evaluation criterion. The following section details the apparent reflectance calculation.

During ultrasonic wave propagation, reflection and transmission typically occur at interfaces between different materials due to acoustic impedance mismatch, accompanied by changes in signal amplitude and phase. When the thicknesses of the media on both sides of the interface are much greater than the ultrasonic wavelength, the reflection and transmission coefficients can be approximated using plane wave theory and are primarily determined by the acoustic impedance of the media. In multi-layer structures, individual layers exhibit distinct acoustic impedance due to variations in material density and sound velocity across the layers [25]. At the steel–epoxy interface, the reflected signal is received by the transducer, and multiple echoes are generated as the ultrasonic waves undergo repeated reflections between the upper and lower boundaries of the medium [26]. Since these multiple reflections occur within the medium, the signals contain rich information about the bonded interface. The

Table I. Acoustic impedance of different materials [29]

Material	Density (Kg/m ³)	Longitudinal wave velocity (m/s)	Acoustic impedance (kg/(m ² ·s))
Steel	7800	5900	46×10^6
Air	1.2	340	408
Epoxy	1200	2337	2.8×10^6

presence of disbond defects alters the acoustic pressure reflectance, which is primarily manifested as variations in echo energy [27]. In practice, direct measurement of the reflectance is challenging because the transmitted energy is unknown [28]. Instead, it is proposed to measure the apparent reflectance r_a , estimated as the ratio of the reflection amplitude at the steel–epoxy interface to that at the steel–air interface. The acoustic impedance of air, steel, and epoxy are shown in Table I. The calculated reflection coefficients at the steel–epoxy and steel–air interfaces are -0.88 and -1 , respectively. A threshold of 0.88 is applied to identify disbond in the tested regions of the steel–epoxy structure. In real applications, the reflection amplitude of ultrasonic A-scan signals from a steel–air interface can be measured through a calibration experiment, and the apparent reflectance r_a can then be obtained accordingly [28].

$$r_a = \frac{A}{A_{ref}}, \quad (11)$$

where A represents the amplitude of the interface reflection signal of a steel–epoxy interface to be measured and A_{ref} represents the amplitude of the interface reflection signal from a steel–air interface, where the thickness of the steel is

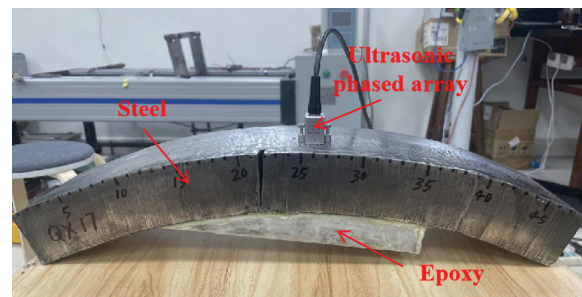


Fig. 3. Experimental setup.

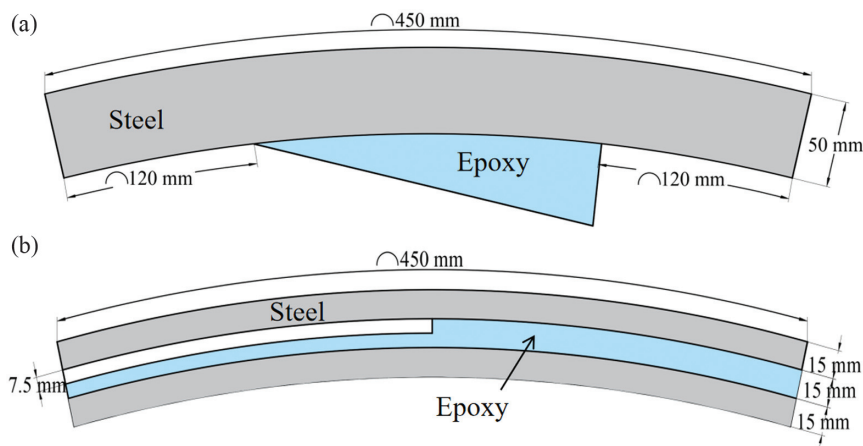


Fig. 2. Configurations of (a) Specimen 1 and (b) Specimen 2.

Table II. Ultrasonic phased array parameters

Probe parameters	Probe
Number of arrays	32
Center frequency	5 MHz
Array spacing	0.6 mm
Array width	10 mm
Relative bandwidth (-6dB)	≥60%
Homogeneity in sensitivity	±2 dB

the same as that of the steel layer in the steel-epoxy structure under investigation. To reduce errors caused by manual operation during the experiment, the ultrasonic signal was normalized by using the amplitude of the second echo for calculation.

III. EXPERIMENTAL PROCEDURE

A. SPECIMEN

Two steel-epoxy structures are used in this paper. The first layer in Specimen 1 is steel with a thickness of 50 mm and

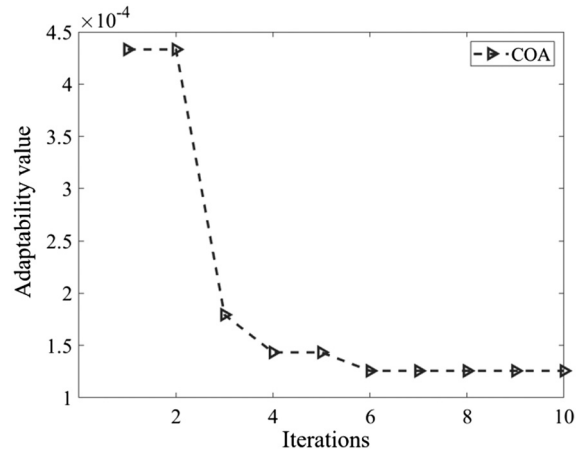


Fig. 4. Fitness function curve.

an arc length of 450 mm, with different thicknesses of epoxy attached in the center (arc length of 210 mm), and air at both ends (arc length of 120 mm, respectively). The

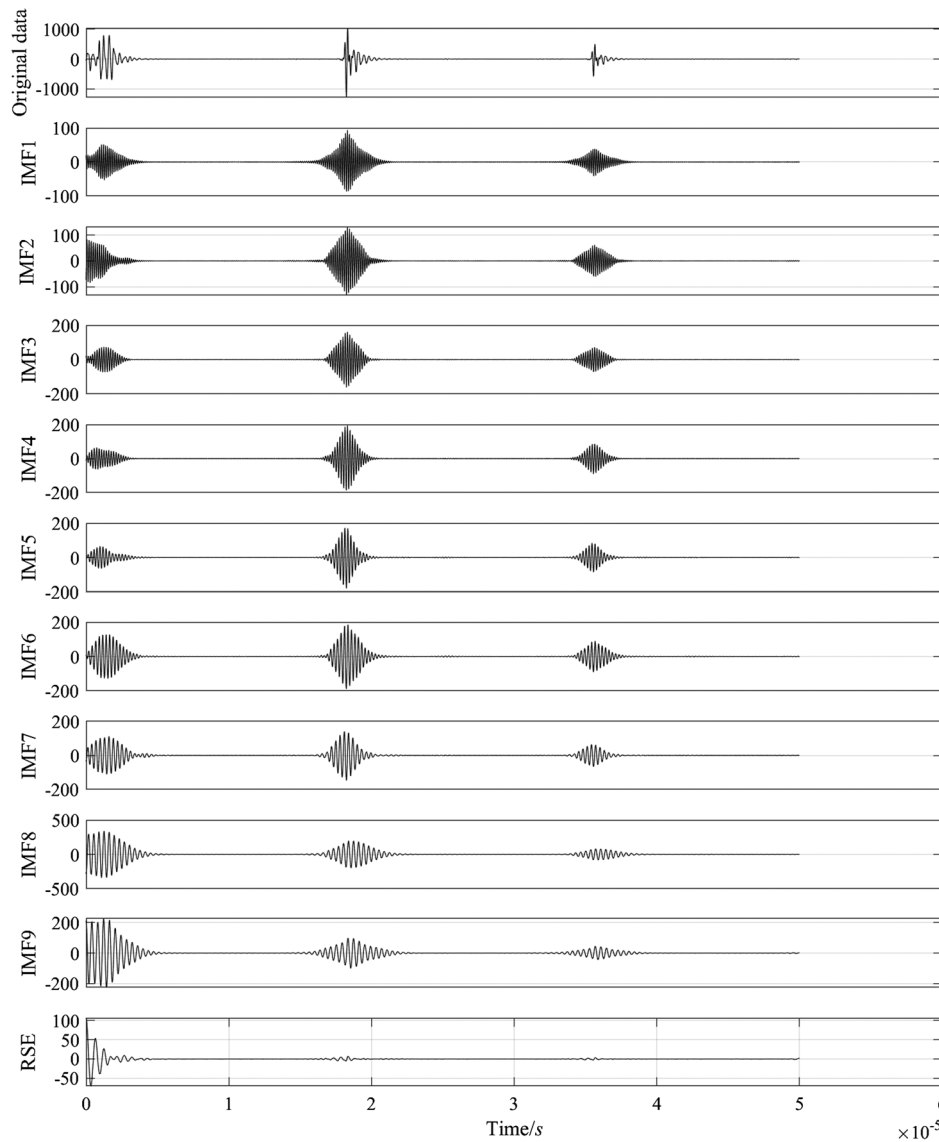


Fig. 5. Ultrasonic time-domain signals processed by VMD at region 1.

configuration is shown in Fig. 2(a). Specimen 2 is a steel pipe with a diameter of 813 mm, a part of which was selected for testing in the configuration shown in Fig. 2(b). The first layer of steel has a thickness of 15 mm and an arc length of 450 mm, and the second layer is an epoxy with a thickness of 15 mm, containing a disbond defect with a thickness of 7.5 mm and an arc length of 225 mm; the third layer of steel also has a thickness of 15 mm. In addition, to determine the apparent reflectance, a corresponding calibration experiment is required. A steel specimen with the same material and dimensions as the first layer is used for calibration, and the normalized echo amplitudes of each signal are obtained and averaged to serve as A_{ref} .

B. EXPERIMENTAL SETUP

The experimental setup is shown in Fig. 3, where an ultrasonic phased array device is used to inspect the steel-epoxy sandwich structures. The experiment was carried out using a 64-channel phased array ultrasonic testing device manufactured by TPAC (France). The phased array ultrasonic probe (Doppler, China) is a 32-element linear

probe with a center frequency of 5 MHz, an element spacing of 0.6 mm, and a sampling frequency of 50 MHz, with detailed parameters listed in Table II. This probe was positioned on the steel surface with its scanning direction aligned parallel to the axis. Consistent contact pressure was maintained throughout the experiments, the aperture number was set to 8, and the gain was set to 15 dB using the line scanning mode. For both Specimen 1 and Specimen 2, 12 uniformly distributed sampling regions were tested on each specimen. For the calibration specimen, three uniformly distributed regions were sampled and measured using the same experimental setups.

IV. EXPERIMENTAL RESULTS

A. SPECIMEN 1

The COA algorithm is performed to optimize the VMD. The population size of COA is set to 20, and the maximum number of iterations is 10. The optimization range for the penalty factor α is from 100 to 3500, and the range for the number of decomposition modes K is from 2 to 15. Using

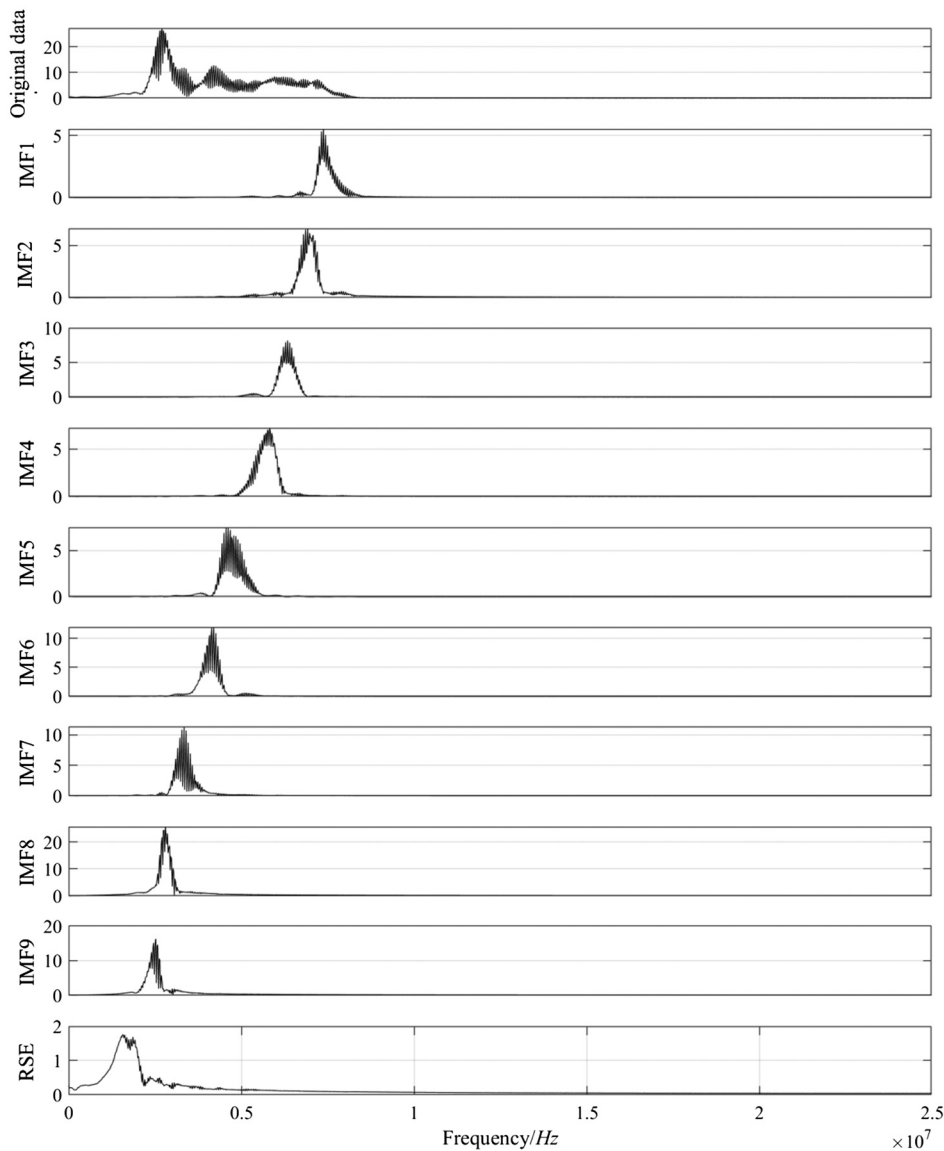


Fig. 6. Ultrasonic frequency-domain signals processed by VMD at region 1.

the ultrasonic data at region 1 of Specimen 1 as an example, the COA optimization results are shown in Fig. 4, where the fitness value (minimum envelope entropy) converged to 1.3×10^{-4} by the 6th iteration. The optimal solution is then preserved and exported, with the corresponding parameters $K=9$ and $\alpha=208$. Based on this optimal parameter combination, VMD decomposition yields 9 IMFs. The time-domain ultrasonic signals and frequency spectra of each IMF are shown in Figs. 5 and 6, respectively. The correlation of each IMF with the original signal was calculated using equation (10), as shown in Table III. IMF 7 was selected and normalized to calculate the apparent reflectance, which exhibits the highest correlation with the original ultrasonic A-scan signals.

The A_{ref} before and after COA-VMD algorithm was calculated to be 0.49 and 0.48, respectively. The apparent reflectance of the ultrasonic signals acquired from Specimen 1 was then calculated using equation (11). The experimental results are presented in Fig. 7(b), where the echo reflectance ratio of the unprocessed signal exhibits significant fluctuations (ranging from 0.45 to 1.1) across the 12 detection regions, with notable misclassification occurring particularly at the defect edge (detection region 6). This suggests that while disbond defects at the steel–epoxy interface can be identified using relative reflectance, some detection errors persist due to the influence of noise and overlap of boundary echo signals. In contrast, after

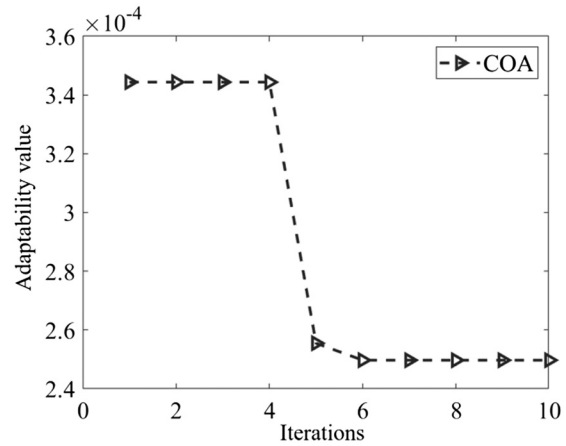


Fig. 8. Fitness function curve.

COA-VMD processing, the apparent reflectance distribution becomes more uniform, and the previously misclassified region is corrected, thereby enhancing the accuracy of ultrasonic disbond defect detection, as shown in Fig. 7(c). This improvement can be attributed to COA-VMD’s ability to retain signal components that are highly correlated with the original ultrasonic signal while suppressing

Table III. Correlation coefficient between each IMF and the original signal

Intrinsic mode function	IMF1	IMF2	IMF3	IMF4	IMF5	IMF6	IMF7	IMF8	IMF9
Correlation coefficient value	0.256	0.305	0.331	0.328	0.395	0.412	0.682	0.482	0.173

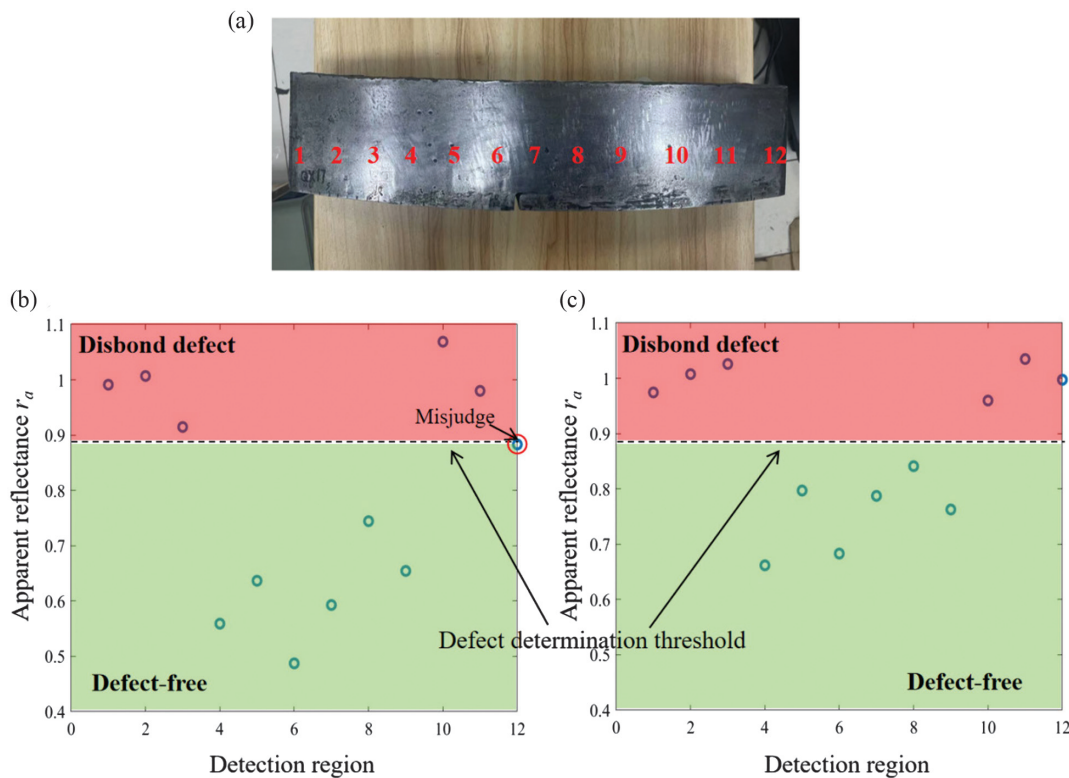


Fig. 7. Defect identification results based on the apparent reflectance threshold: (a) the test specimen is divided into 12 regions, (b) defect characterization results of the original ultrasonic A-scan signals, and (c) defect characterization results of the COA-VMD processed ultrasonic signals.

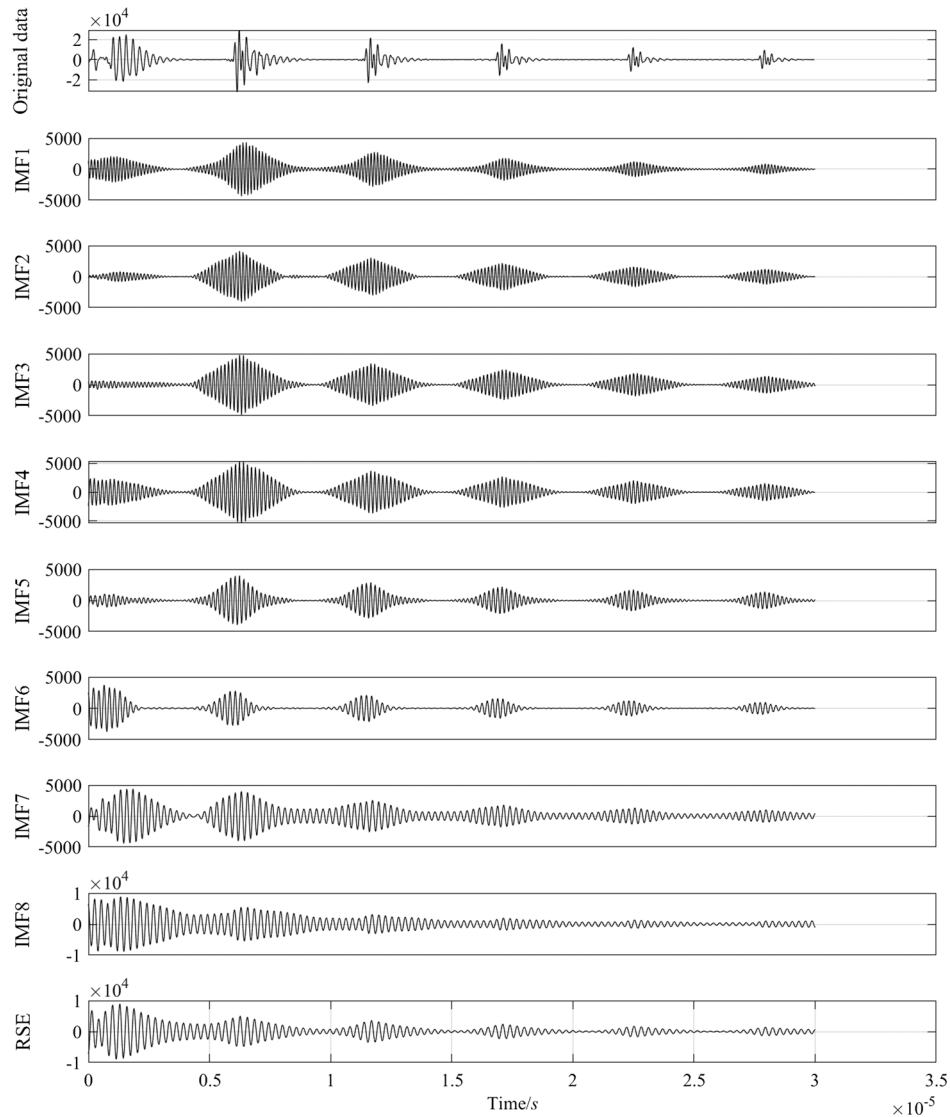


Fig. 9. Ultrasonic time-domain signals processed by VMD at region 1.

high-frequency noise components with low correlation, thus improving the overall quality of the ultrasonic signal.

B. SPECIMEN 2

To further demonstrate the capability of the COA-VMD and apparent reflectance algorithm for disbond defect detection, Specimen 2 with different thicknesses is used. For detection region 1 of Specimen 2, Fig. 8 shows the results of COA optimization with a goodness of fit value of 2.5×10^{-4} for the 6th iteration. After calculating $K = 8$ and $\alpha = 1500$, the decomposition is obtained by bringing in the VMD as shown in Figs. 9 and 10. The IMF correlation results are shown in Table IV, where it can be seen that IMF 7 has the highest correlation with the original ultrasonic signal.

The values of A_{ref} before and after COA-VMD processing were calculated to be 0.72 and 0.67, respectively. Similarly, the apparent reflectance r_a of the ultrasonic signal obtained from specimen 2 and of the ultrasonic signal after COA-VMD calculation was calculated using equation (11).

Figure 11(b) presents the disbond defect detection results for the unprocessed signal. The amplitude ratio of the untreated signal shows large fluctuations within a certain range, and misclassification is observed in region 5, primarily due to noise interference and the superposition of transverse wave signals on the secondary returned longitudinal waves. After COA-VMD processing, however, the distribution of the apparent reflectance becomes more consistent, and the misclassification in region 5 is corrected, as illustrated in Fig. 11(c). These results demonstrate that COA-VMD effectively extracts high-quality ultrasonic signals from sandwich structures with variable thicknesses and enhances the accuracy of disbond defect detection. The improved apparent reflectance profiles further confirm COA-VMD's ability to suppress overlapping echoes and environmental noise, which is essential for accurate defect localization. Overall, the successful application of this method to Specimen 2 reinforces the versatility and reliability of the proposed ultrasonic surface reflectance-based approach for detecting disbond defects in sandwich structures.

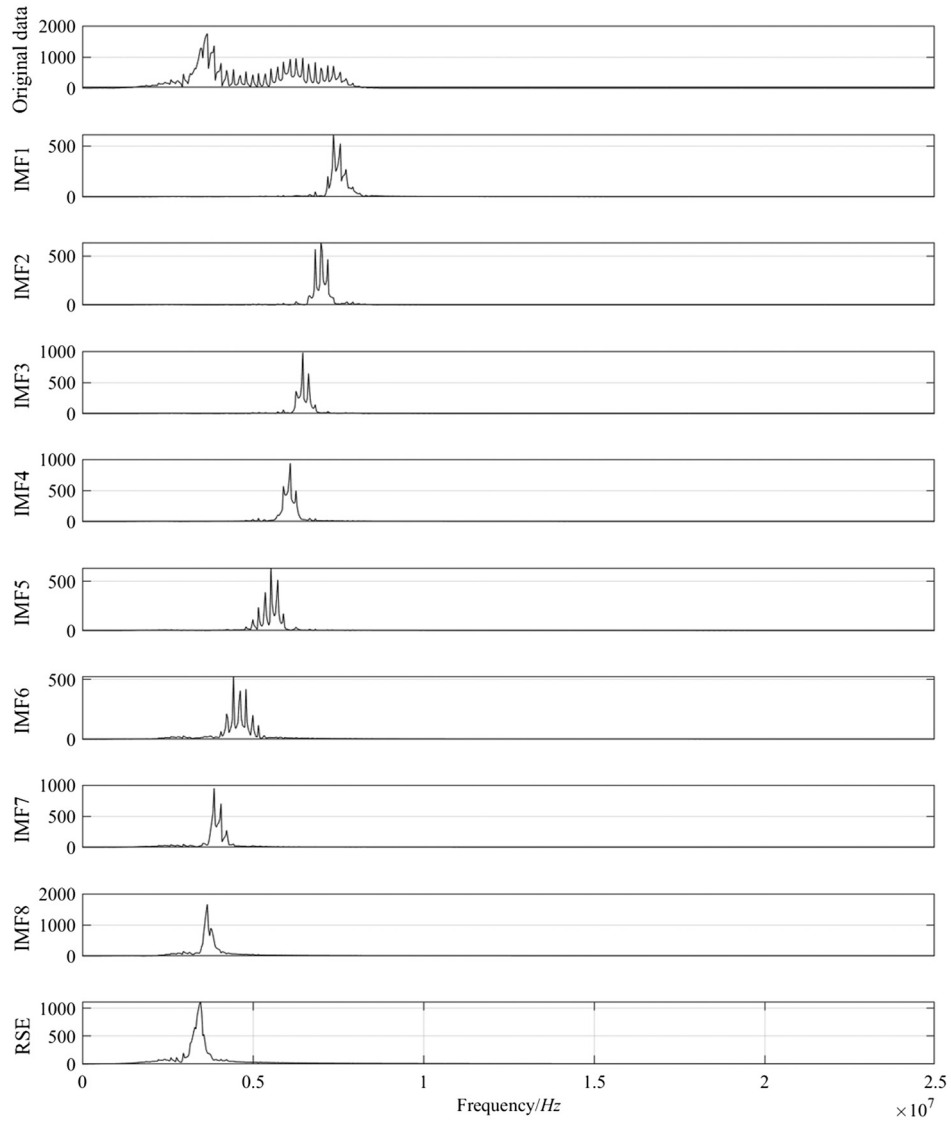


Fig. 10. Ultrasonic frequency-domain signals processed by VMD at region1.

Table IV. Correlation coefficient between each IMF and the original signal

Intrinsic mode function	IMF1	IMF2	IMF3	IMF4	IMF5	IMF6	IMF7	IMF8
Correlation coefficient value	0.261	0.297	0.356	0.361	0.252	0.362	0.641	0.535

V. DISCUSSIONS

The COA-VMD algorithm demonstrates significant advancements in detecting disbond defects in steel-epoxy-steel sandwich structures. Compared to conventional manual parameter tuning methods, the automation of K and α selection reduces subjectivity and improves detection repeatability, which is critical for industrial applications requiring standardized quality assessments. By adaptively optimizing VMD parameters through the COA, this approach effectively suppresses noise interference and aliased echoes, as evidenced by the stabilized apparent reflectance distributions in both Specimen 1 and Specimen 2. However, the method

has some limitations that require further investigation. First, while the algorithm effectively localizes the disbond regions, it cannot quantify additional characteristics such as the thickness of the disbond layers. This limits its applicability in scenarios that require quantitative defect severity assessment, such as evaluating residual structural strength. Second, the current experimental validation is based on two-dimensional testing methods applied to steel-epoxy composite structures with predefined defect geometries. The performance of this method on irregularly shaped defects or materials with complex acoustic properties, as well as its extension to three-dimensional detection, remains untested.

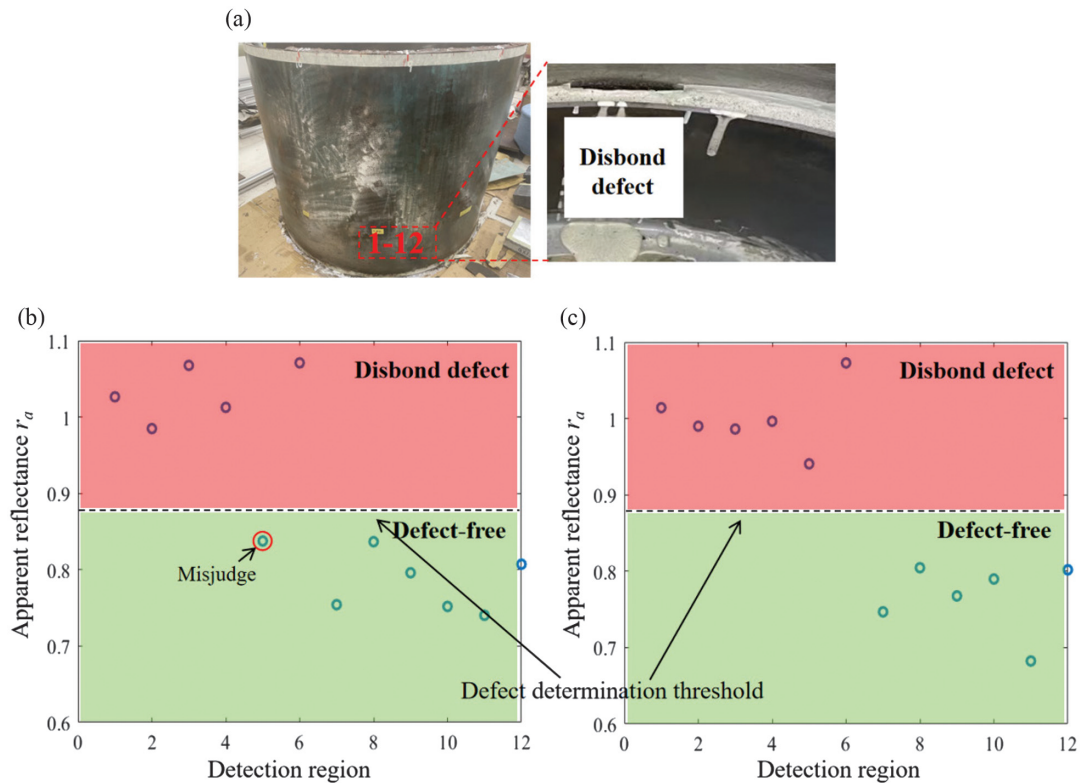


Fig. 11. Defect identification results based on the apparent reflectance threshold: (a) the test specimen is divided into 12 regions, (b) defect characterization results of the original ultrasonic A-scan signals, and (c) defect characterization results of the COA-VMD processed ultrasonic signals.

VI. CONCLUSION

In this study, an ultrasonic detection method for disbond defects in steel-epoxy-steel sandwich structures is proposed. To address the challenge of low detection accuracy of ultrasonic disbond defects, a parameter-adaptive optimization algorithm based on COA-VMD is introduced. The COA autonomously determines the optimal VMD parameters, specifically the penalty factor and the number of decomposition modes, using the minimum envelope entropy as the fitness function. This effectively minimizes the inaccuracies introduced by manual parameter adjustments. After extracting the IMFs with the highest correlation coefficient to the ultrasonic signals, the apparent reflectance is calculated to establish a quantitative evaluation index of the interface state. This index, based on the acoustic impedance discontinuity at the material interface, enables the identification of disbond defects. Experiment results show that this method can locate the disbond defects in steel-epoxy structures.

ACKNOWLEDGEMENTS

This work was supported by the Research Funding of Hangzhou International Innovation Institute of Beihang University (Grant No. 015731201-2024KQ126), National Key R&D Program of China (Grant No. 2023YFF0716600), and National Natural Science Foundation of China (Grant No. 62271021).

REFERENCES

- [1] U. Bahaman, Z. Mustafa, M. E. A. B. Seghier, and T. M. Badri, "Evaluating the reliability and integrity of composite pipelines in the oil and gas sector: a scientometric and systematic analysis," *Ocean Eng.*, vol. 303, p. 117773, 2024.
- [2] A. Algolfat, W. Wang, and A. Albarbar, "Damage identification of wind turbine blades—a brief review," *J. Dyn. Monit. Diagn.*, vol. 2, no. 1, pp. 198–206, 2023.
- [3] H. Guo, R. Li, L. Sun, S. Chen, and H. Miao, "Inspecting epoxy layer defects in steel-epoxy-steel sandwich structures using guided waves," *Measurement*, vol. 231, p. 114551, 2024.
- [4] M. Mehdikhani, L. Gorbatikh, I. Verpoest, and S. V. Lomov, "Voids in fiber-reinforced polymer composites: a review on their formation, characteristics, and effects on mechanical performance," *J. Compos. Mater.*, vol. 53, no. 12, pp. 1579–1669, 2019.
- [5] D. Borrie, S. Al-Saadi, X. L. Zhao, R. S. Raman, and Y. Bai, "Bonded CFRP/steel systems, remedies of bond degradation and behaviour of CFRP repaired steel: an overview," *Polymers (Basel)*, vol. 13, no. 9, pp. 1533, 2021.
- [6] Z. Xiao, J. Rao, S. Eisenträger, K. V. Yuen, and S. A. Hadigheh, "Generative adversarial network-based ultrasonic full waveform inversion for high-density polyethylene structures," *Mech. Syst. Signal Process.*, vol. 224, p. 112160, 2025.
- [7] J. Rao, J. Yang, J. He, M. Huang, and E. Rank, "Elastic least-squares reverse-time migration with density variation for flaw imaging in heterogeneous structures," *Smart Mater. Struct.*, vol. 29, no. 3, p. 035017, 2020.
- [8] J. S. Popovics and K. V. Subramaniam, "Review of ultrasonic wave reflection applied to early-age concrete and cementitious materials," *J. Nondestruct. Eval.*, vol. 34, pp. 1–12, 2015.
- [9] X. Wang, J. Wang, G. Shen, X. Li, and Z. Huang, "Research on interface bonding characteristics of layered medium using

- ultrasonic oblique incidence,” *Compos. Struct.*, vol. 295, p. 115733, 2022.
- [10] H. Hou, J. Li, S. Xia, Y. Meng, and J. Shen, “Ultrasonic resonance-based inspection of ultra-thin nickel sheets bonded to silicone,” *Mater. Res. Express.*, vol. 10, no. 4, p. 046502, 2023.
- [11] S. A. Titov, R. G. Maev, and A. N. Bogachenkov, “Pulse-echo NDT of adhesively bonded joints in automotive assemblies,” *Ultrasonics*, vol. 48, no. 6–7, pp. 537–546, 2008.
- [12] J. Chen, Y. Shi, and S. Shi, “Noise analysis of digital ultrasonic nondestructive evaluation system,” *Int. J. Press. Vessel Pip.*, vol. 76, no. 9, pp. 619–630, 1999.
- [13] R. Huang, J. Xia, B. Zhang, Z. Chen, and W. Li, “Compound fault diagnosis for rotating machinery: state-of-the-art, challenges, and opportunities,” *J. Dyn. Monit. Diagn.*, vol. 2, no. 1, pp. 13–29, 2023.
- [14] J. Lian, Z. Liu, H. Wang, and X. Dong, “Adaptive variational mode decomposition method for signal processing based on mode characteristic,” *Mech. Syst. Signal Process.*, vol. 107, pp. 53–77, 2018.
- [15] Y. Wang, R. Markert, J. Xiang, and W. Zheng, “Research on variational mode decomposition and its application in detecting rub-impact fault of the rotor system,” *Mech. Syst. Signal Process.*, vol. 60, pp. 243–251, 2015.
- [16] H. Li, S. Li, J. Sun, B. Huang, J. Zhang, and M. Gao, “Ultrasound signal processing based on joint GWO-VMD wavelet threshold functions,” *Measurement*, vol. 226, p. 114143, 2024.
- [17] F. Xu, Y. Wu, H. Lin, Y. Liu, X. Wang, R. J. Ross, and G. Tian, “IPSO-VMD based signal feature extraction and internal defect detection of hardwood logs through acoustic impact test,” *NDT E Int.*, vol. 139, p. 102942, 2023.
- [18] M. Dehghani, Z. Montazeri, E. Trojovská, and P. Trojovský, “Coati optimization algorithm: a new bio-inspired metaheuristic algorithm for solving optimization problems,” *Knowl.-Based Syst.*, vol. 259, p. 110011, 2023.
- [19] Y. Zhao, C. Li, W. Fu, J. Liu, T. Yu, and H. Chen, “A modified variational mode decomposition method based on envelope nesting and multi-criteria evaluation,” *J. Sound Vib.*, vol. 468, p. 115099, 2020.
- [20] Y. Zhou, J. Lu, Z. Hu, H. Dong, W. Yan, and D. Yang, “Novel feature extraction method of pipeline signals based on multi-scale dispersion entropy partial mean of multi-modal component,” *Measurement*, vol. 205, p. 112137, 2022.
- [21] K. Dragomiretskiy and D. Zosso, “Variational mode decomposition,” *IEEE Trans. Signal Process.*, vol. 62, no. 3, pp. 531–544, 2013.
- [22] X. Zhang, Q. Miao, H. Zhang, and L. Wang, “A parameter-adaptive VMD method based on grasshopper optimization algorithm to analyze vibration signals from rotating machinery,” *Mech. Syst. Signal Process.*, vol. 108, pp. 58–72, 2018.
- [23] A. D. Woodbury and T. J. Ulrych, “Minimum relative entropy: Forward probabilistic modeling,” *Water Resour. Res.*, vol. 29, no. 8, pp. 2847–2860, 1993.
- [24] Y. Shen, W. Zheng, W. Yin, A. Xu, and H. Zhu, “Feature extraction algorithm using a correlation coefficient combined with the VMD and its application to the GPS and GRACE,” *IEEE Access*, vol. 9, pp. 17507–17519, 2021.
- [25] M. R. Zarastvand, M. Ghassabi, and R. Talebitooti, “Prediction of acoustic wave transmission features of the multilayered plate constructions: a review,” *J. Sandw. Struct. Mater.*, vol. 24, no. 1, pp. 218–293, 2022.
- [26] L. Goglio and M. Rossetto, “Ultrasonic testing of adhesive bonds of thin metal sheets,” *NDT E Int.*, vol. 32, no. 6, pp. 323–331, 1999.
- [27] W. Li and H. Hu, “Reflection and transmission of plane waves in stressed media with an imperfectly bonded interface,” *Geophys. J. Int.*, vol. 233, no. 3, pp. 2233–2253, 2023.
- [28] H. Liu, Z. Chen, Y. Liu, Y. Chen, Y. Du, and F. Zhou, “Interfacial debonding detection for CFST structures using an ultrasonic phased array: application to the Shenzhen SEG building,” *Mech. Syst. Signal Process.*, vol. 192, p. 110214, 2023.
- [29] N. Hiremath, V. Kumar, N. Motahari, and D. Shukla, “An overview of acoustic impedance measurement techniques and future prospects,” *Metrol.*, vol. 1, no. 1, pp. 17–38, 2021.